J Mater Sci (2018) 53:15418–15429

Chemical routes to materials

Syntheses and ultra-deep desulfurization performance of sandwich-type polyoxometalate-based TiO_2 nanofibres

Jiawei Fu[1], Yu Guo[1], Wenwen Ma[1,2,*], Chen Fu[1], Li Li[1], Haiyu Wang[1], and Hong Zhang[1,*]

[1] *Institute of Polyoxometalate Chemistry, Department of Chemistry, Northeast Normal University, Changchun 130024, Jilin, People's Republic of China*

[2] *College of Chemistry and Chemical Engineering, Shenyang Normal University, Shenyang 110034, Liaoning, People's Republic of China*

Received: 15 May 2018
Accepted: 23 July 2018
Published online: 2 August 2018

ABSTRACT

The sandwich-type polyoxometalate-based TiO_2 nanofibres were prepared successfully by electrospinning combining with chemical reaction and employed in ultra-deep desulfurization. OTA–CoVW–TiO_2 nanofibres (OTA = $CH_3(CH_2)_{17}(CH_3)_3N$, CoVW = $[Co_4(H_2O)_2(VW_9O_{34})_2]^{10-}$) confirmed the excellent desulfurization performance in extraction catalytic oxidative desulfurization system (ECODS). At 323 K, the 500 ppm DBT (dibenzothiophene) model oil was entirely removed within 20 min using 0.010 g 45 wt% OTA–CoVW–TiO_2 nanofibres as catalyst when O/S molar ratio was 4:1 and the dosage of model oil was 5 mL. The catalysts could be recycled and reused at least five times without remarkable decrease in catalytic activity. The desulfurization efficiencies for different substrates were shown as following order: DBT > 4,6-DMDBT (4,6-dimethyl-dibenzothiophene) > BT (benzothiophene). Moreover, the possible mechanism was also elucidated.

Introduction

SO_x emissions not only result in environmental pollution, but also do harm to human health during the combustion of sulfur compounds in fuels [1, 2]. Consequently, it is attractive to address the practical challenge of reducing sulfur content in fuels to ultra-low levels according to the stringent regulations imposed by governments [3]. Hydrodesulphurization (HDS) is deemed as a kind of current desulfurization technology in refineries [4]. However, trace amounts of sulfur compounds make ultra-deep desulfurization extremely tough at the expense because of some harsh operational conditions, for instance, the higher temperature (300–400 °C) and pressure (20–100 atm of H_2), more efficient catalysts or longer residence times [5]. Especially, it is less effective for that of heterocyclic sulfur compounds in HDS [6, 30]. Hence, different desulfurization methods have been extensively investigated including

Address correspondence to E-mail: mwwbhu@sina.com; hope20130122@163.com; zhangh@nenu.edu.cn

https://doi.org/10.1007/s10853-018-2736-z

oxidative desulfurization (ODS), bio-desulfurization (BDS) and extractive desulfurization (EDS) [7, 9, 13, 15]. Combining extractive desulfurization and oxidative desulfurization makes contribution to the development of ECODS, a one-pot environmental benignity desulfurization technology, which can remove refractory sulfur-containing compounds effectively under mild conditions [8, 9]. The effectiveness of ECODS process crucially depends on the choice of appropriate oxidant, extractant and catalyst. The desulfurization process was carried out using various oxidants such as H_2O_2 [10], molecular oxygen [11] and organic peroxide [12]. H_2O_2 is considered as the most economical and effective oxidant among all oxidants [13]. In addition, ionic liquids (ILs) have been verified as environmental friendly extractant instead of conventional organic solvents and play a role in stabilizing active centers in ECODS [3, 14]. Consequently, exploring and preparing a kind of efficient catalyst for ECODS is the particular task for obtaining the little-to-no sulfur concentration fuels.

Polyoxometalates (POMs) are a series of transition metal oxygen clusters, the remarkable advantages of which are unique properties, rich structural versatility and widespread application value [15–17]. Sandwich-type POMs are comprised of fragments $[XW_9O_{34}]^{n-}$ (X = transition metal), which have been employed in many aspects [13, 18, 20] so far, including water oxidation [19], photocatalysis [20] and desulfurization . [13, 21, 22]. The desulfurization systems of pure POMs as catalysts are not undesirable for practical industrial applications due to poor reusability; thus, heterogeneous catalysts are regarded as an advanced quest in this regard to solve these problems. More attention has been paid to immobilize POMs on various supports, such as SiO_2 [23, 24], TiO_2 [25, 26, 30] and active carbon [27]. The evident advantages of TiO_2 as support have been verified and employed in various fields [20, 28], and the desulfurization application is of particular interest. On the one hand, the active sites on the surface of TiO_2 are capable to absorb the atom with lone pair electrons, which is conducive to desulfurization process since there are lone pair electrons on sulfur [26, 29, 30]. On the other hand, the utilization efficiency of H_2O_2 can benefit from the hydrophilic feature of TiO_2 [30]. In addition, the phase structure of TiO_2 is a fatal parameter that affects the desulfurization efficiency according to the report that the desulfurization performance enhanced with the POMs combining with anatase TiO_2 [31]. Moreover, 18.2% desulfurization efficiency of anatase–rutile phase TiO_2 was obtained in photocatalytic oxidation [32]. Up to now, there are few reports about the sandwich-type polyoxometalate-based TiO_2 nanofibres with the mixed-phase of anatase–rutile phase as catalysts and employed in ultra-deep desulfurization.

In this work, OTA–CoVW–TiO_2 nanofibres (OTA = $CH_3(CH_2)_{17}(CH_3)_3N$, CoVW = $[Co_4(H_2O)_2(VW_9O_{34})_2]^{10-}$) were synthesized via electrospinning combining with chemical reaction and presented the excellent desulfurization performance. The morphology and structure of catalysts were characterized by field emission scanning electron microscopy (FE-SEM), energy dispersion spectroscopy (EDS) and X-ray diffractometry (XRD) etc. Meanwhile, the influence factors of desulfurization were systematically investigated and optimal conditions were obtained. The reusability for catalysts was researched, and the mechanism of ECODS was also studied.

Materials and methods

Chemicals

Vanadate(V)-centered polyoxometalate $Na_{10}[Co_4(H_2O)_2(VW_9O_{34})_2]\cdot 35H_2O$ and $(OTA)_{10}[Co_4(H_2O)_2(VW_9O_{34})_2]$ were prepared and the fabrication process was shown in "Supplementary Material." 1-Butyl-3-methyl imidazolium hexafluorophosphate ([Bmim]PF_6) was synthesized according to the literature [33]. *N*,*N*-dimethylformamide (DMF, AR, Tianjin Tiantai Chemical Co. Ltd.), acetic acid (AR, Beijing Chemical Works), Tetrabutyl titanate ($Ti(OC_4H_9)_4$, TBOT, 99%, Tianjin GuangFu Fine Chemical Research Institute), acetylacetone (99%, Xilong Chemical Co. Ltd.), polyvinyl pyrrolidone (PVP, M_W = 1300000, Aladdin), dodecyltrimethylammonium bromide (DTA·Br, 99%, Energy Chemical), hexadecyltrimethylammonium bromide (HTA·Br, 99%, Energy Chemical), octadecyltrimethylammonium chloride (OTA·Cl, 99%, Energy Chemical), dioctadecyldimethylammonium chloride (DDA·Cl, 99%, Energy Chemical), hydrogen peroxide (H_2O_2, 30 wt%, Beijing Chemical Works), benzothiophene (BT, 99%, China Pingmei Shenma Energy & Chemical Group Co., Ltd.),

dibenzothiophene (DBT, 99%, China Pingmei Shenma Energy & Chemical Group Co., Ltd.), 4,6-dimethyl-dibenzothiophene (4,6-DMDBT, 99%, China Pingmei Shenma Energy & Chemical Group Co., Ltd.), dichloromethane (Tianjin GuangFu Fine Chemical Research Institute) and *n*-octane (Tianjin GuangFu Fine Chemical Research Institute), and biphenyl (Sinopharm Chemical Reagent Co., Ltd.) were directly used as received without further purification.

Preparation of catalysts

The synthetic process of TiO_2 nanofibres was presented in "Supplementary Material." In the typical procedure of preparing representative 45 wt% OTA–CoVW–TiO_2 nanofibres, 0.100 g TiO_2 nanofibres was dispersed in 50.000 mL ethanol and stirred magnetically for 30 min before 0.040 g OTA·Cl was added, which was marked solution A. 0.064 g $Na_{10}[Co_4(H_2O)_2(VW_9O_{34})_2]\cdot 35H_2O$ was dissolved in 20.000 mL H_2O and marked as solution B. Then solution B was drop-wise added into solution A with stirring rapidly and continuously for 24 h. Finally the precipitations were filtered and washed with water and ethanol before drying at 80 °C. The sample was obtained and denoted as 45-OTA–CoVW–TiO_2 NF (45 wt% OTA–CoVW–TiO_2 nanofibres). All catalysts were synthesized with similar process. 45-DDA–CoVW–TiO_2 NF: 45 wt% DDA–CoVW–TiO_2 nanofibres; 45-DTA–CoVW–TiO_2 NF: 45 wt% DTA–CoVW–TiO_2 nanofibres; 45-HTA–CoVW–TiO_2 NF: 45 wt% HTA–CoVW–TiO_2 nanofibres; 25-OTA–CoVW–TiO_2 NF: 25 wt% OTA–CoVW–TiO_2 nanofibres; 35-OTA–CoVW–TiO_2 NF: 35 wt% OTA–CoVW–TiO_2 nanofibres; 55-OTA–CoVW–TiO_2 NF: 55 wt% OTA–CoVW–TiO_2 nanofibres.

Desulfurization experiments

Model oils with a corresponding sulfur content of 500 ppm were prepared by dissolving BT, DBT and 4,6-DMDBT in *n*-octane, respectively, and biphenyl was standard substance. 5 mL model oil was put in a 50-mL round bottom flask, which was immerged in temperature-controlling water bath and stirred 15 min constantly at a certain temperature. And then 1 mL IL ([Bmim]PF_6), definitive amount of H_2O_2 and catalysts were added in turn. The upper layer of oil was analyzed on gas chromatography (GC). The temperature was fixed at 303, 313, 323 and 343 K. The dosage of catalyst was 0.005, 0.010, 0.015 and 0.020 g. And the O/S molar ratio was 2:1, 3:1, 4:1 and 6:1.

Characteristics

The infrared (FT-IR) absorption spectra were examined with KBr Pelles on a Mattson Alpha-Centauri Fourier transform infrared spectrometer, and the range was fixed in 4000–400 cm^{-1} with the number of scan 64 and the resolution 4 cm^{-1}. X-ray photoelectron spectroscopy (XPS) measurements were performed with a ThermoFisher ESCALAB250 X-ray photoelectron spectrometer (powered at 150 W) using Al Kα radiation. Thermogravimetric analysis (TG) was implemented on a Perkin-Elmer Thermal Analyzer under nitrogen atmosphere at a heating rate of 10 °C min^{-1}, and the temperature was raised from 15 to 600 °C. XRD analysis was investigated using a Rigaku D/Max-RA X-ray diffractometer in the 2θ range from 5° to 80° with Cu Kα radiation. The morphology of the catalyst was measured by Hitachi SU8010 field emission scanning electron microscope (FE-SEM). Under a working voltage of 200 kV, transmission electron microscope (TEM) analysis was employed using a JEM-2010 transmission electron microscope, images were obtained digitally on Gatan multiople CCD camera. The elemental analysis and mapping of product were carried out using OXFORD ISIS-300 energy-dispersive spectrometer. The Brunauer–Emmett–Teller (BET) specific surface areas and pore structures were performed by a Micromeritics V-Sorb 2800P. The loading amount of OTA–CoVW was supported on TiO_2 nanofibres, which was resolved by a Leeman Prodigy Spec inductively coupled plasma atomic emission spectrometer (ICP-AES). The Agilent 7820A-GC System using DB-5 chromatographic column with 30 m × 0.32 mm × 0.25 μm was employed to GC analysis, and the measurements were adjusted as follows: injection port temperature was 200 °C, detector temperature was 250 °C, and 150 °C was immobilized as oven temperature. Ultra-pure nitrogen was fixed as carrier gas. The injection volume of sample was 1 μL. The desulfurization efficiency was calculated by internal standard method.

Results and discussion

Catalysts characterization

The FT-IR spectra of OTA·Cl, $Na_{10}[Co_4(H_2O)_2(VW_9O_{34})_2]\cdot 35H_2O$ and 45-OTA–CoVW–TiO_2 NF are shown in Fig. 1. The bands at 2850 and 2915 cm^{-1} are attributed to OTA^+ in OTA·Cl (Fig. 1a). The representative peaks in 2700–3000 cm^{-1} are identified as C–H stretching modes for the cations of carbon chain quaternary ammonium salt [34]. From Fig. 1b, we can see that $Na_{10}[Co_4(H_2O)_2(VW_9O_{34})_2]\cdot 35H_2O$ shows characteristic peaks at 955 and 861 cm^{-1}, which are assigned to the asymmetric vibrations of V–O and W=O, respectively. The peaks of 812 and 667 cm^{-1} are caused by corner-/edge-sharing W–O–W bending [35]. Figure 1c displays that these similar characteristic peaks of $[Co_4(H_2O)_2(VW_9O_{34})_2]^{10-}$ in 45-OTA–CoVW–TiO_2 NF. However, their vibrational frequencies change to 960, 867, 817 and 673 cm^{-1}. The result is attributed by the strong interaction between the $[Co_4(H_2O)_2(VW_9O_{34})_2]^{10-}$ and TiO_2 support at the interface of the two components [3]. Moreover, there are no obvious new vibrational signal other than that of OTA·Cl and $[Co_4(H_2O)_2(VW_9O_{34})_2]^{10-}$ in the FT-IR spectra of 25-OTA–CoVW–TiO_2 NF, 35-OTA–CoVW–TiO_2 NF and 55-OTA–CoVW–TiO_2 NF (Fig. S1), meaning that the intact structure of sandwich-type POMs for these catalysts is still retained.

As shown in Fig. 2, 25-OTA–CoVW–TiO_2 NF, 35-OTA–CoVW–TiO_2 NF, 45-OTA–CoVW–TiO_2 NF and 55-OTA–CoVW–TiO_2 NF not only emerge representative diffraction peaks of rutile TiO_2 (PDF#75-1749), but also present the peaks of anatase TiO_2 (PDF#71-1166) in the scope of 2θ from 5° to 80°, reflecting the phase structure of these catalysts is the mixed-phase of rutile and anatase. Notably, the same structure of bare TiO_2 nanofibres, 45-DDA–CoVW–TiO_2 NF, 45-DTA–CoVW–TiO_2 NF, 45-HTA–CoVW–TiO_2 NF and 45-OTA–CoVW–TiO_2 NF is observed in Fig. S2, implying the structure of catalysts is unchanged with various loading amounts of OTA–CoVW and cations containing various carbon chain lengths. The successful preparation of these catalysts is verified adequately combining FT-IR and XRD analysis. Moreover, it is mentioned that Co, V, W, C, O and Ti elements are included in EDS spectrum of 45-OTA–CoVW–TiO_2 NF (Fig. S3).

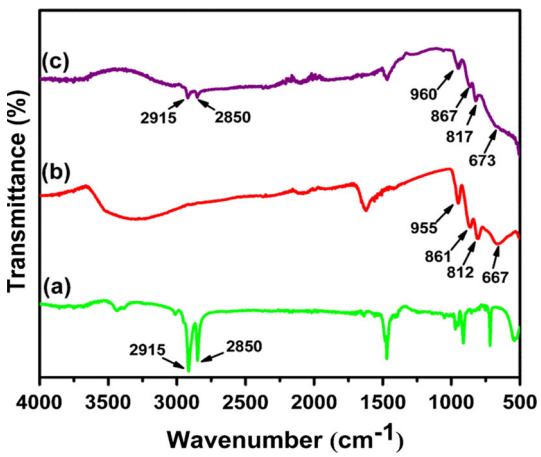

Figure 1 The FT-IR spectra of (a) OTA·Cl, (b) $Na_{10}[Co_4(H_2O)_2(VW_9O_{34})_2]\cdot 35H_2O$, (c) 45-OTA–CoVW–$TiO_2$ NF.

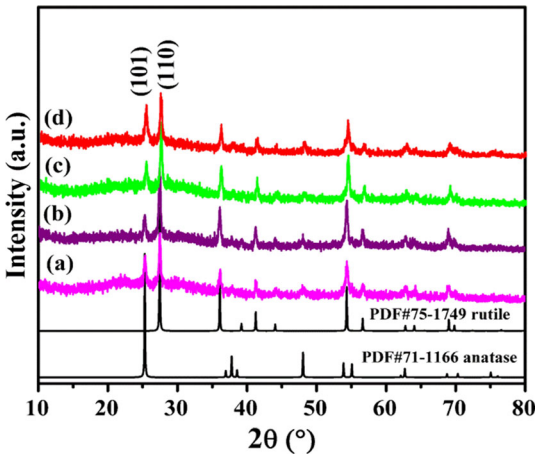

Figure 2 XRD patterns of (a) 25-OTA–CoVW–TiO_2 NF, (b) 35-OTA–CoVW–TiO_2 NF, (c) 45-OTA–CoVW–TiO_2 NF and (d) 55-OTA–CoVW–TiO_2 NF with the standard cards of anatase and rutile phase TiO_2.

The XPS analysis is used to further study the chemical composition and oxidation state in 45-OTA–CoVW–TiO_2 NF. The curve fitting of Co 2*p* is resolved into four peaks (Fig. 3a), the binding energies of about 779.4 and 784.3 eV are assigned to Co $2p_{3/2}$, and the XPS signals of 795.7 and 802 eV are contributed by Co $2p_{1/2}$, respectively. Co in 45-OTA–CoVW–TiO_2 NF is established to be Co(III) [36]. The peak of 528.8 eV is associated with V $2p_{3/2}$ (Fig. 3b). V(III) is in the catalyst [37]. Furthermore, the spectrum of Fig. 3c presents the binding energies at 34.2 and 36.3 eV, which are attributed to W $f_{7/2}$ and W $f_{5/2}$, respectively. The result confirms the presence of W(VI) [38]. Two peaks of 457.5 and 463.3 eV are observed in Fig. 3d, which are caused by Ti $2p_{3/2}$ and Ti $2p_{1/2}$, respectively. Ti(IV) is in the catalyst [39]. The

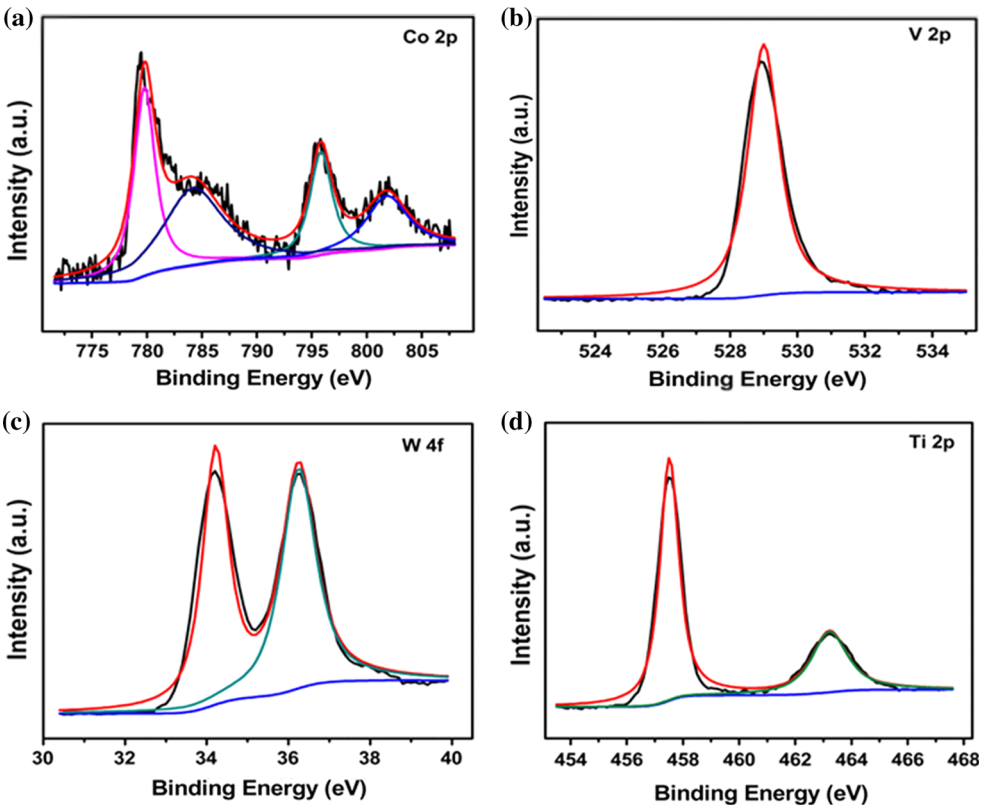

Figure 3 XPS spectra of 45-OTA–CoVW–TiO_2 NF, **a** Co 2*p*, **b** V 2*p*, **c** W 4*f* and **d** Ti 2*p*.

results of XPS agree well with the EDS analysis and further prove that OTA–CoVW is indeed supported on TiO_2 nanofibres in 45-OTA–CoVW–TiO_2 NF.

To identify the morphology of the supported catalyst, FE-SEM is taken on 45-OTA–CoVW–TiO_2 NF. The uniform fiber-like is scattered evenly in the ambient environment (Fig. 4a). From Fig. 4b, we can catch sight of the large areas of TiO_2 nanofibres are occupied by many evident black spots, revealing that the active species are uniformly distributed on the surface of TiO_2 nanofibres, which may be beneficial to accelerate the desulfurization efficiency [40]. The OTA–CoVW and TiO_2 nanofibres are distinguished immediately by HR-TEM (Fig. 4c). As can be observed in Fig. 5, the excellent dispersity of OTA–CoVW on TiO_2 nanofibres is approved by elemental mapping. The result illustrates that Co, V, W, C, O and Ti are contained in 45-OTA–CoVW–TiO_2 NF, which is good accordance with the TEM analysis. Furthermore, the decompositions of 45-OTA–CoVW–TiO_2 NF at different temperatures are investigated by TGA analysis (Fig. S4) and the corresponding demonstrations are shown in "Supplementary Material," which provides the evidence for the excellent stability.

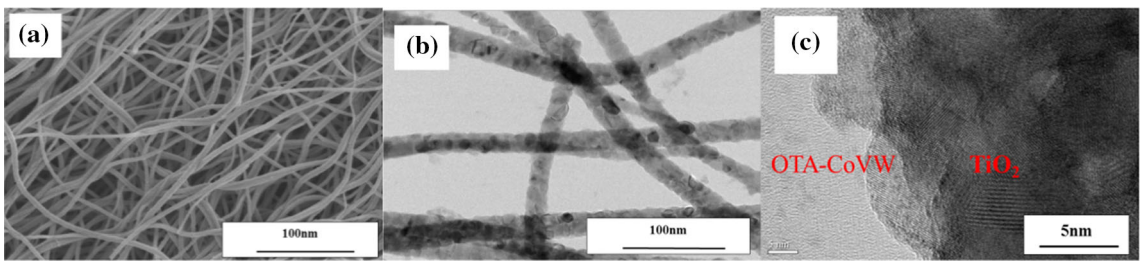

Figure 4 **a** FE-SEM image of 45-OTA–CoVW–TiO_2 NF, **b** TEM image of 45-OTA–CoVW–TiO_2 NF, **c** HR-TEM image of 45-OTA–CoVW–TiO_2 NF.

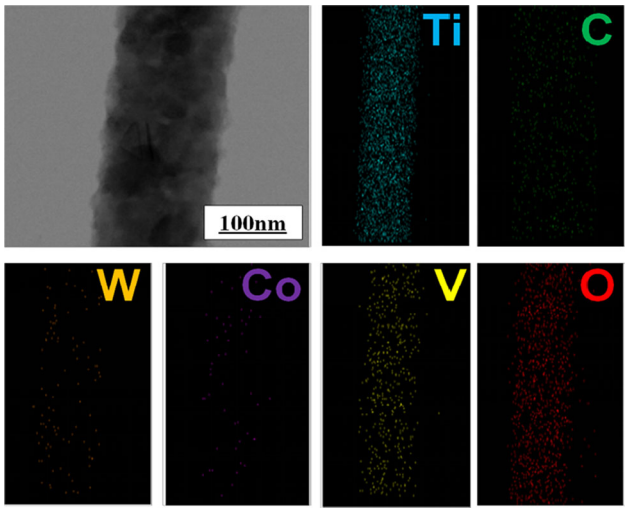

Figure 5 The TEM image of signal nanofiber of 45-OTA–CoVW–TiO_2 NF and corresponding elemental mapping of Ti (cyan), C (green), W (orange), Co (purple), V (yellow) and O (red) on 45-OTA–CoVW–TiO_2 NF.

The impact on desulfurization efficiency of various desulfurization systems and catalysts

It is instructive to compare the desulfurization efficiency for different desulfurization systems. As shown in Entry 1–5 of Table 1, DBT removal efficiency for ODS (Entry 1), EDS (Entry 2), oxidative catalytic desulfurization system (OCDS, Entry 3), extractive catalytic desulfurization system (ECDS, Entry 4) and ECODS (Entry 5) were 4, 14, 14, 33 and 100%, respectively. The higher desulfurization efficiency of ECODS was owed to the coordination effect among H_2O_2, IL ([Bmim]PF_6) and catalysts.

The impact on desulfurization efficiency of various catalysts was investigated, and the results are listed in Entry 6–8 of Table 1. A total of 31, 66 and 0.7% desulfurization efficiency was obtained in 20 min using CoVW, OTA–CoVW and TiO_2 nanofibres as catalyst, respectively. DBT removal efficiency of 0.7% was ascribed to the poor adsorptive capacity of TiO_2 nanofibres [41]. It was noteworthy that 45-OTA–CoVW–TiO_2 NF could efficiently decrease the DBT concentration under mild conditions comparing to previous reports (Table S1). Thus, 45-OTA–CoVW–TiO_2 NF was the most appropriate catalyst in ECODS for investigating other influential factors during the whole desulfurization process.

The influence of POMs with different cations in catalysts on desulfurization efficiency

As could be observed in Fig. 6, it took 90, 60, 40 and 20 min to achieve 100% desulfurization efficiency using 45-DDA–CoVW–TiO_2 NF, 45-DTA–CoVW–TiO_2 NF, 45-HTA–CoVW–TiO_2 NF and 45-OTA–CoVW–TiO_2 NF as catalyst, respectively. The poorer catalytic activity of 45-DDA–CoVW–TiO_2 NF with double-carbon chain was assigned to the relatively strong stereo-effect, which made the active species hard to approach H_2O_2 [9, 42, 43]. Additionally, the desulfurization efficiency was also influenced by the length of the carbon chain for the catalyst with single-alkyl chain [44]. The desulfurization performance of 45-OTA–CoVW–TiO_2 NF was superior to that of 45-DTA–CoVW–TiO_2 NF and 45-HTA–CoVW–TiO_2 NF obviously, since a dual trap for both DBT and H_2O_2 was provided by the catalyst with long single-alkyl chain [45]. It is favorable to affirm the optimum catalyst for removing DBT was 45-OTA–CoVW–TiO_2 NF.

Table 1 Desulfurization efficiency of various desulfurization systems and catalysts

Entry	Catalysts	Oxidant	Extractant	Desulfurization efficiency (%)
1	No	H_2O_2	No	4
2	No	No	[Bmim]PF_6	14
3	45-OTA–CoVW–TiO_2 NF	H_2O_2	No	14
4	45-OTA–CoVW–TiO_2 NF	No	[Bmim]PF_6	33
5	45-OTA–CoVW–TiO_2 NF	H_2O_2	[Bmim]PF_6	100
6	[a]CoVW	H_2O_2	[Bmim]PF_6	31
7	[b]OTA–CoVW	H_2O_2	[Bmim]PF_6	66
8	[c]TiO_2 nanofibres	H_2O_2	[Bmim]PF_6	0.7

Reaction conditions: T = 323 K, m_{cat} = 0.010 g, O/S = 4:1, t = 20 min

[a]CoVW: $Na_{10}[Co_4(H_2O)_2(VW_9O_{34})_2]\cdot 35H_2O$, [b]OTA–CoVW: $(OTA)_{10}[Co_4(H_2O)_2(VW_9O_{34})_2]$ and [c]TiO_2 nanofibres: the preparation process was presented in "Supplementary Material"

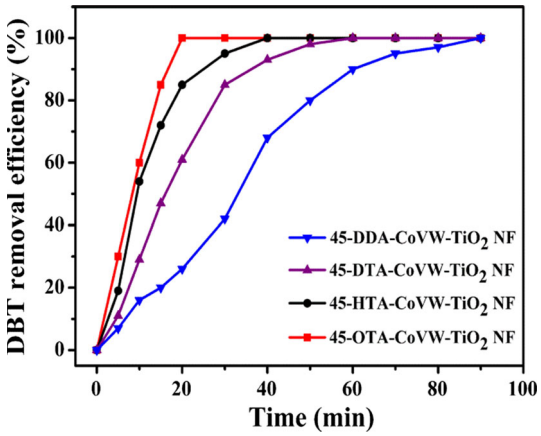

Figure 6 The influence of POMs with different cations in catalysts on desulfurization efficiency, reaction conditions: T = 323 K, m_{cat} = 0.010 g, O/S = 4:1.

The impact of loading amount of OTA–CoVW and catalyst dosage on desulfurization efficiency

The catalytic activity of catalysts mainly depended on the amount of active species, which was limited by the loading amount of OTA–CoVW and the dosage of catalysts. Figure 7a displayed that 97% desulfurization efficiency was obtained with 25-OTA–CoVW–TiO_2 NF in 90 min, while 60, 20 and 80 min were consumed to achieve 100% DBT removal efficiency using 35-OTA–CoVW–TiO_2 NF, 45-OTA–CoVW–TiO_2 NF and 55-OTA–CoVW–TiO_2 NF as catalyst, respectively. The real loading amounts of OTA–CoVW on TiO_2 nanofibres were measured by ICP, and the calculated results are shown in Table S2, which indicated that the loading amounts of OTA–CoVW in 45-OTA–CoVW–TiO_2 NF were approximate equal to the original added amounts, which contributed a large amount of available active sites (peroxo-POMs) for polyoxometalate-based catalysts [29]. Below 45 wt% of OTA–CoVW concentration, the low amounts of active centers were not enough to catalysis sulfur compound entirely. Meanwhile, the distribution of active species also had a vital impact on desulfurization efficiency [46, 47]. Hence, the BET surface area and pore volume of 45-OTA–CoVW–TiO_2 NF were researched and the results are listed in Table S3, the higher DBT conversion efficiency of 45-OTA–CoVW–TiO_2 NF was attributed by the possibility that many pores were occupied by more POMs, which not only reduced BET surface area and exposed more active sites, the interference was obtained by the TEM analysis of 45-OTA–CoVW–TiO_2 NF.

45-OTA–CoVW–TiO_2 NF with superior desulfurization performance was the suitable catalyst to investigate the impact of catalyst dosage on desulfurization efficiency. Figure 7b highlighted that the desulfurization efficiency was 79% using 0.005 g catalyst within 90 min, while 100% DBT removal efficiency was obtained during 20, 40 and 70 min when the dosage of catalyst was 0.010, 0.015 and 0.020 g, respectively. The excess catalysts possibly led to the aggregation of nanofibres, which covered on the surface of the catalyst and decreased the amounts of defective sites available. According to above analysis, we concluded that the desulfurization performance of 45-OTA–CoVW–TiO_2 NF was the most outstanding when the dosage of catalyst was 0.010 g.

The influence of reaction temperature on desulfurization efficiency

As could be seen in Fig. 8, 79% desulfurization efficiency was reached in 90 min at 303 K, the required operational time for complete removal of DBT reduced from 60 to 20 min when the temperature increased from 313 to 323 K, respectively, implying

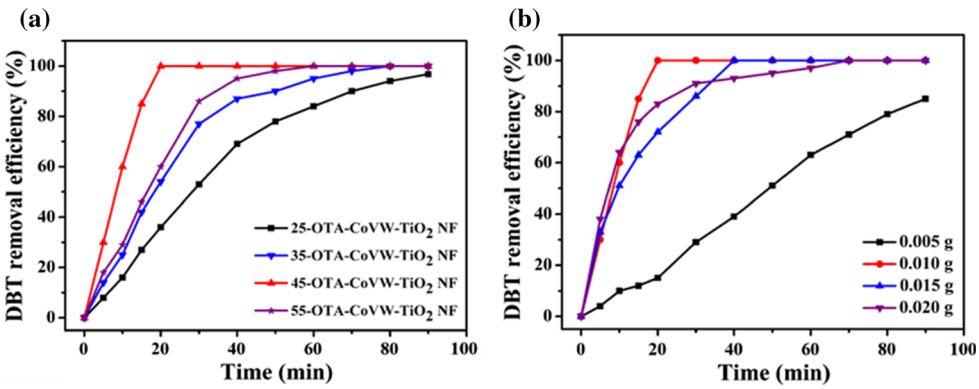

Figure 7 **a** The impact of loading amount of OTA–CoVW on desulfurization efficiency, reaction conditions: O/S = 4:1, m_{cat} = 0.010 g, T = 323 K; **b** the impact of 45-OTA–CoVW–TiO_2 NF catalyst dosage on desulfurization efficiency, reaction conditions: O/S = 4:1, T = 323 K.

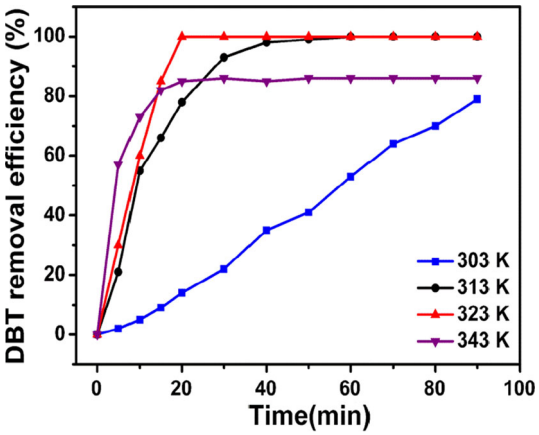

Figure 8 The influence of reaction temperature on desulfurization efficiency for 45-OTA–CoVW–TiO_2 NF, reaction conditions: O/S = 4:1, m_{cat} = 0.010 g.

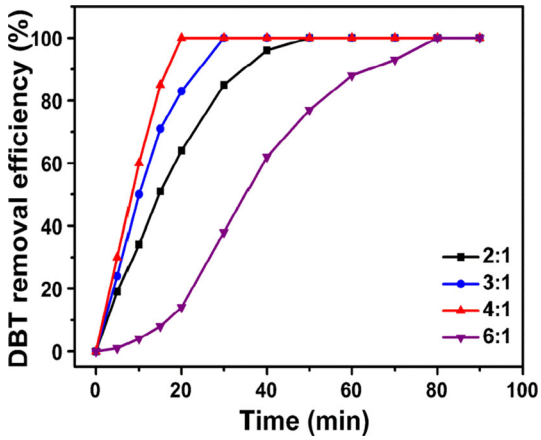

Figure 9 The effect of O/S molar ratio on DBT removal efficiency for 45-OTA–CoVW–TiO_2 NF, reaction conditions: T = 323 K, m_{cat} = 0.010 g.

the desulfurization performance enhanced with the increasing of temperature. However, when the temperature was elevated to 343 K, the reaction time for 86% DBT removal efficiency could be prolonged to 90 min. This was probably due to more H_2O_2 self-decomposition under higher temperature [48, 49]. Therefore, 323 K was the optimum temperature for the requirement of deep desulfurization.

The effect of O/S molar ratio on DBT removal efficiency

The H_2O_2/DBT molar ratio (O/S) has a vital effect on DBT removal efficiency and economy of the desulfurization system; thus, various O/S molar ratios were examined in ECODS and the results are shown in Fig. 9. The required time to achieve 100% DBT removal efficiency could be shorten from 80 to 20 min when the O/S molar ratio decreased from 6:1 to 4:1, respectively. Below 4:1 of O/S molar ratio, 100% desulfurization efficiency was achieved more than 20 min. Stoichiometrically, 1 mol sulfur compound is oxidized to corresponding sulfone with 2 mol H_2O_2 [50, 51]. In this work, 4:1 was the optimal O/S molar ratio, which was higher than the stoichiometric value. The result was assigned to the competing reaction of the oxidation that nonproductive decomposition of H_2O_2 itself [52]. Consequently, more H_2O_2 was needed to generate peroxo-POMs for the oxidation of DBT. Nevertheless, further increasing O/S molar ratio from 4:1 to 6:1 led to more aqueous solution in the system, which was responsible for decreasing the concentration of active species and reducing DBT removal efficiency. Accordingly, 4:1 was the most appropriate O/S molar ratio and applied in the current desulfurization process.

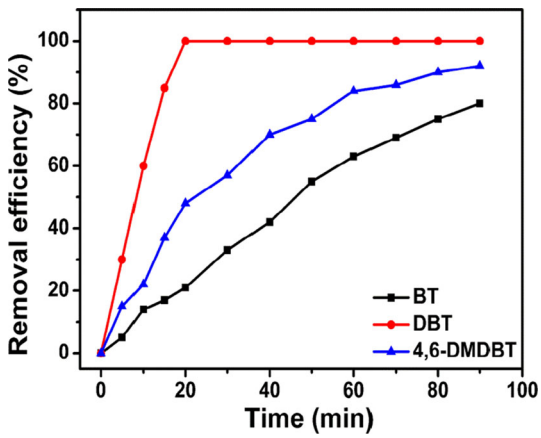

Figure 10 Desulfurization efficiencies on different substrates with 45-OTA–CoVW–TiO_2 NF, reaction conditions: T = 323 K, m_{cat} = 0.010 g, O/S = 4:1.

Desulfurization efficiencies on different substrates

Considering the potential industrial application value and the compatibility of 45-OTA–CoVW–TiO_2 NF, BT and 4,6-DMDBT were also inflexible to be transformed into corresponding sulfones and necessary to be evaluated. Figure 10 displayed that the desulfurization efficiency of BT, 4,6-DMDBT and DBT was 79, 92 and 100% in 90, 90 and 20 min, respectively. The removal efficiency of various substrates was mainly affected by electron density of S-atom and steric

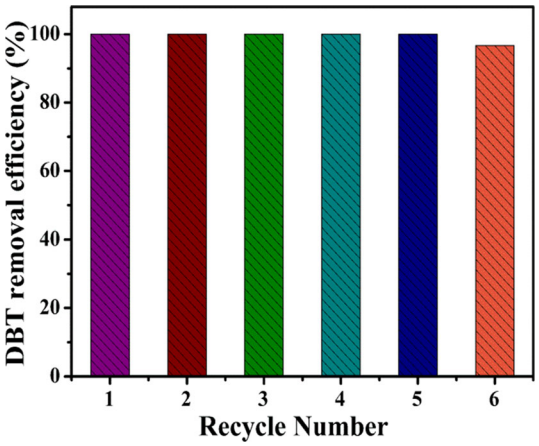

Figure 11 Recycle performance of 45-OTA–CoVW–TiO_2 NF, reaction conditions: T = 323 K, m_{cat} = 0.010 g, O/S = 4:1.

hindrance. The desulfurization efficiency of BT (5.568) was lower than DBT (5.758), which was attributed to electron density, steric hindrance was caused by methyl without consideration [9, 48]. The electron densities of 4,6-DMDBT (5.760) and DBT were approximate, but the desulfurization efficiency of DBT far exceed that of 4,6-DMDBT corresponding to the negative approaching S-atom from the two methyl groups on the benzene ring of 4,6-DMDBT.

Recycling

The reusability of catalyst is a significant respect to industrial application, and the recyclable performance of 45-OTA–CoVW–TiO_2 NF was experimented under the optimum conditions. Decantation was employed to separate oil from IL phase since they were immiscible. The oil was poured out carefully after the first run, and remnants were washed with appropriate dichloromethane and then dried at 80 °C in an oven. Afterward, H_2O_2 and fresh model oil were added for the next run. As shown in Fig. 11, the desulfurization efficiency only decreased from 100 to 97% after recycling for five times. The accumulation of $DBTO_2$ formed an obstacle between active sites and sulfur compounds, which was considered as the main parameter for the slight decrease in DBT conversion efficiency [48, 53]. Above all, 45-OTA–CoVW–TiO_2 NF could be recycling at least five times for deeply desulfurization.

Mechanism

To acquire a better understanding of the excellent desulfurization performance, the proposed desulfurization mechanism of 45-OTA–CoVW–TiO_2 NF in ECODS was studied. The ECODS was consisted of three phases: DBT was included in the oil phase and lived in the upper layer, the middle phase contained oxidative agent (H_2O_2) and IL phase with dispersive catalysts was the lowest layer. Three phases could fully contact with each other under the magnetic stirring. More and more peroxo-POMs [$W(O_2)$] were obtained by reacting with H_2O_2 because of the hydrophilic characteristic of POMs, and the hydrophobic property of carbon chain

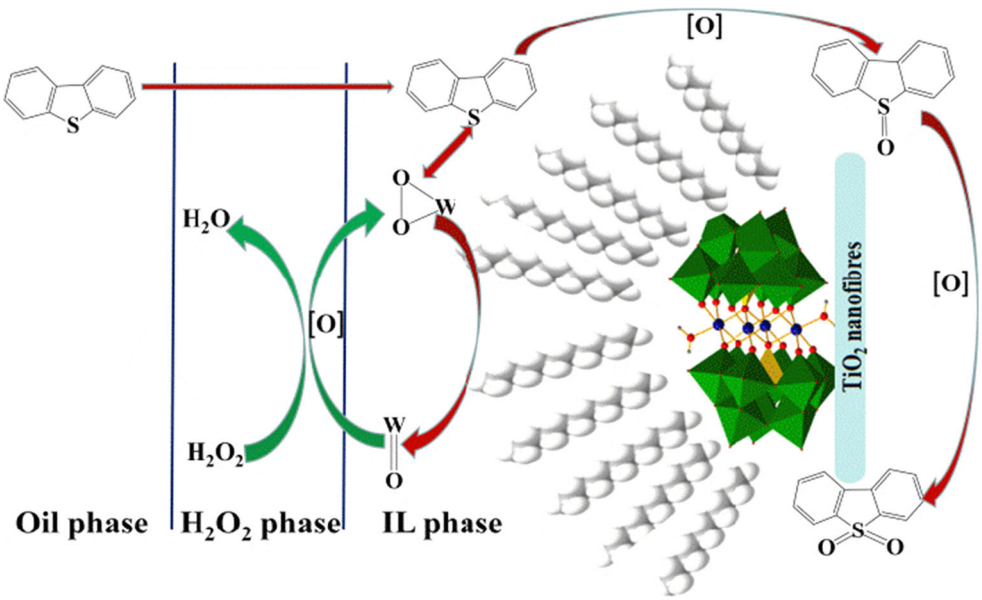

Figure 12 Proposed desulfurization mechanism of 45-OTA–CoVW–TiO_2 NF in ECODS with three liquid-phase systems.

made it easy to approach DBT [13, 42, 44]. Hence, the amphiphilic heterogeneous catalysts with the higher catalytic activity were recycled and reused conveniently. As shown in Fig. 12, [Bmim]PF_6 extracted DBT to IL phase firstly [3], the active peroxo species W (O_2) were formed via reacting between W=O and H_2O_2 simultaneously. W(O_2) provided [O] to the oxidation of DBT, and the preliminary production DBTO was further oxidized to $DBTO_2$. Finally, the higher polar $DBTO_2$ was retained in the IL phase [8, 27] resulting in a continuous decrease in DBT concentration in the oil. It was noteworthy that the active peroxo species W(O_2) returned back to W=O continuously, which was forced to stop until H_2O_2 exhausted fully [30].

Conclusions

In this work, various catalysts were prepared successfully by electrospinning combining with chemical reaction and employed in desulfurization process. 500 ppm DBT model oil could be entirely removed using 0.010 g 45-OTA–CoVW–TiO_2 NF as catalyst and [Bmim]PF_6 as extractant at 323 K in 20 min, when the dosage of model oil was 5 mL and O/S molar ratio was 4:1. Moreover, the desulfurization efficiencies for different substrates decreased in the order of DBT > 4,6-DMDBT > BT. The last but not least, the catalysts could be easily regenerated and reused for five consecutive cycles with unnoticeable decrease in catalytic activity indicating the excellent practical industrial application prospect.

Acknowledgements

This work was financially supported by the NSF of China (21271038, 21571032) and the China High-Tech Development 863 Program (2007AA03Z218). Furthermore, the Northeast Normal University provided the excellent platform of testing and gave us help seasonable.

Electronic supplementary material: The online version of this article (https://doi.org/10.1007/s10853-018-2736-z) contains supplementary material, which is available to authorized users.

References

[1] Zhang J, Zhao DH, Yang LY, Li YB (2010) Photocatalytic oxidation dibenzothiophene using TS-1. Chem Eng J 156:528–531

[2] Zhang J, Wang AJ, Wang YJ, Wang HY, Gui JZ (2014) Heterogeneous oxidative desulfurization of diesel oil by hydrogen peroxide: catalysis of an amphipathic hybrid material supported on SiO_2. Chem Eng J 245:65–70

[3] Ma WW, Xu Y, Ma KW, Zhang H (2016) Electrospinning synthesis of $H_3PW_{12}O_{40}/TiO_2$ nanofiber catalytic materials and their application in ultra-deep desulfurization. Appl Catal A Gen 526:147–154

[4] Jiang X, Li HM, Zhu WS, He LN, Shu HM, Lu JD (2009) Deep desulfurization of fuels catalyzed by surfactant-type decatungstates using H_2O_2 as oxidant. Fuel 88:431–436

[5] Otsuki SJ, Nonaka TS, Takashima N, Qian WH, Ishihara AS, Imai TT, Kabe T (2000) Oxidative desulfurization of light gas oil and vacuum gas oil by oxidation and solvent extraction. Energy Fuel 14:1232–1239

[6] Banisharif F, Reza Dehghani M, Capel-Sanchez M, Campos-Martin JM (2017) Desulfurization of fuel by extraction and catalytic oxidation using a vanadium substituted Dawson-type emulsion catalyst. Ind Eng Chem Res 56:3839–3852

[7] Ramos JM, Wang JA, Chen LF, Arellano U, Ramirez SP, Sotelo R, Schachat P (2015) Synthesis and catalytic evaluation of CoMo/SBA-15 catalysts for oxidative removal of dibenzothiophene from a model diesel. Catal Commun 72:57–62

[8] Zhu WS, Li HM, Jiang X, Yan YS, Lu JD, He LN, Xia JX (2008) Commercially available molybdic compound-catalyzed ultra-deep desulfurization of fuels in ionic liquids. Green Chem 10:641–646

[9] Li HM, Zhu WS, Wang Y, Zhang JT, Lu JD, Yan YS (2009) Deep oxidative desulfurization of fuels in redox ionic liquids based on iron chloride. Green Chem 11:810–815

[10] Xun SH, Zhu WS, Zhu FX, Chang YH, Zheng D, Qin YJ, Zhang M, Jiang W, Li HM (2015) Design and synthesis of W-containing mesoporous material with excellent catalytic activity for the oxidation of 4,6-DMDBT in fuels. Chem Eng J 280:256–264

[11] Tang NF, Zhang YN, Lin F, Lv HY, Jiang ZX, Li C (2012) Oxidation of dibenzothiophene catalyzed by [$C_8H_{17}N(CH_3)_3H_3V_{10}O_{28}$] using molecular oxygen as oxidant. Chem Commun 48:11647–11649

[12] Filippis PD, Scarsella M (2003) Oxidatie desulfurization: oxidation reactivity of sulfur compounds in different organic matrixes. Energy Fuel 17:1452–1455

[13] Xu Y, Ma WW, Dolo A, Zhang H (2016) An amphiphilic catalyst based on sandwich-type polyoxometalate for deep

desulfurization of fuels in ionic liquid. RSC Adv 6:66841–66846

[14] Li HM, Jiang X, Zhu WS, Lu JD, Shu HM, Yan YS (2016) Deep oxidative desulfurization of fuel oils catalyzed by decatungstates in the ionic liquid of [Bmim]PF_6. Chem Res 48:9034–9039

[15] Li CP, Li D, Zou SS, Li Z, Yin JM, Wang AL, Cui YN, Yao ZL, Zhao Q (2013) Extraction desulfurization process of fuels with ammonium-based deep eutectic solvents. Green Chem 15:2793–2799

[16] Song J, Luo Z, Britt DK, Furukawa H, Yaghi OM, Hardcastle KI, Hill CL (2011) A multiunit catalyst with synergistic stability and reactivity: a polyoxometalate metal organic framework for aerobic decontamination. J Am Chem Soc 133:16839–16846

[17] Yao ZX, Miras HN, Song YF (2016) Efficient concurrent removal of sulfur and nitrogen contents from complex oil mixtures by using polyoxometalate-based composite materials. Inorg Chem Front 3:1007–1013

[18] Zhou J, Chen WC, Sun CY, Han L, Qin C, Chen MM, Wang XL, Wang EB, Su ZM (2017) Oxidative polyoxometalates modified graphitic carbon nitride for visible-light CO_2 reduction. ACS Appl Mater Interfaces 9:11689–11695

[19] Yin QS, Tan JM, Besson C, Geletii YV, Musaev DG, Kuznetsov AE, Luo Z, Hardcastle KI, Hill CL (2010) A fast soluble carbon-free molecular water oxidation catalyst based on abundant metals. Science 328:342–345

[20] Chen Z, Duan ZY, Wang ZL, Liu XY, Gu L, Zhang FX, Dupuis M, Li C (2017) Amorphous cobalt oxide nanoparticles as active water-oxidation catalysts. ChemCatChem 9:3641–3645

[21] Hong YL, Jing XL, Huang JL, Sun DH, Odoom-Wubah T, Yang F, Du MM, Li QB (2014) Biosynthesized bimetallic Au–Pd nanoparticles supported on TiO_2 for solvent-free oxidation of benzyl alcohol. ACS Sustain Chem Eng 2:1752–1759

[22] Zhang M, Zhu WS, Xun SH, Li HM, Gu QQ, Zhao Z, Wang Q (2013) Deep oxidative desulfurization of dibenzothiophene with POM-based hybrid materials in ionic liquids. Chem Eng J 220:328–336

[23] Qiu JH, Wang GH, Zhang YQ, Zeng DL, Chen Y (2015) Direct synthesis of mesorporous $H_3PMo_{12}O_{40}/SiO_2$ and its catalytic performance in oxidative desulfurization of fuel oil. Fuel 147:195–202

[24] Xun SH, Zhu WS, Zheng D, Zhang L, Li Hu, Yin S, Zhang M, Li HM (2014) Synthesis of metal-based ionic liquid supported catalyst and its application in catalytic oxidative desulfurization of fuels. Fuel 136:358–365

[25] Huang D, Wang YJ, Cui YC, Luo GS (2008) Direct synthesis of mesoporous TiO_2 and its catalytic performance in DBT oxidative desulfurization. Microporous Mesoporous Mater 116:378–385

[26] Xun SH, Zhu WS, Zheng D, Li HP, Jiang W, Zhang M, Qin YJ, Zhao Z, Li HM (2015) Supported ionic liquid [Bmim]$FeCl_4$/Am TiO_2 as an efficient catalyst for the catalytic oxidative desulfurization of fuels. RSC Adv 5:43528–43536

[27] Xiao J, Wu LM, Wu Y, Liu B, Dai L, Li Z, Xia QB, Xi HX (2014) Effect of gasoline composition on oxidative desulfurization using a phosphotungstic acid/activated carbon catalyst with hydrogen peroxide. Appl Energy 113:78–85

[28] Su CY, Ran X, Hu JL, Shao CL (2013) Photocatalytic process of simultaneous desulfurization of fuel gas by TiO_2-polyacrylontrile nanofibers. Environ Sci Technol 47:11562–11568

[29] Liu G, Rodriguez JA, Chang Z, Hrbek J, Gonzalez L (2002) Adsorption of methanethiol on stoichiometric and defective TiO_2 (110) surfaces: a combined experimental and theoretical study. J Phys Chem B 106:9883–9891

[30] Xun SH, Zheng D, Yin S, Qin YJ, Zhang M, Jiang W, Zhu WS, Li HM (2016) TiO_2 microspheres supported polyoxometalate-based ionic liquids induced catalytic oxidative deep-desulfurization. RSC Adv 6:42402–42412

[31] Ma WW, Xu Y, Ma KW, Luo YH, Liu YS, Zhang H (2017) Synthesis of $PW_{11}Sn/TiO_2$ nanofiber catalytic materials with tunable rutile/anatase phase and application in ultra-deep desulfurization. Mol Catal 433:28–36

[32] Li LT, Zhang JS, Shen C, Wang YJ, Luo GS (2016) Oxidative desulfurization of model fuels with pure nano-TiO_2 as catalyst directly without UV irradiation. Fuel 167:9–16

[33] Carda-Broch S, Berthod A, Armstrong DW (2003) Solvent properties of the 1-butyl-3-methylimidazolium hexafluorophosphate ionic liquid. Anal Bioanal Chem 375:191–199

[34] Lv HY, Ren WZ, Liao WP, Chen W, Li Y, Suo ZH (2013) Aerobic oxidative desulfurization of model diesel using a B-type Anderson catalyst $[C_8H_{17}N(CH_3)_2]_3Co(OH)_6Mo_6O_{18}{\cdot}3H_2O$. Appl Catal B Environ 138–139:79–83

[35] Flynn CM, Pope MT (1973) Tungstovanadate heteropoly complexes. IV. Vanadium(IV) complexes. Inorg Chem 12:1626–1634

[36] Tan BJ, Klabunde KJ, Sherwood PMA (1991) XPS studies of solvated metal atom dispersed (SMAD) catalysts evidence for layered cobalt–manganese particles on alumina and silica. J Am Chem Soc 113:855–861

[37] Silversmit G, Depla D, Poelman H, Marin GB, Gryse RD (2004) Determination of the V2*p* XPS binding energies for different oxidation states (V^{5+} to V^{0+}). J Electron Spectrosc 135:167–175

[38] Zhang M, Zhu WS, Li HM, Xun SH, Ding WJ, Liu JJ, Zhao Z, Wang Q (2014) One-pot synthesis characterization and desulfurization of functional mesoporous W-MCM-41 from POM-based ionic liquids. Chem Eng J 243:386–393

[39] Palanisamy B, Badu CM, Sundaravel B, Anandan S, Murugesan V (2013) Sol–gel synthesis of mesoporous mixed Fe_2O_3/TiO_2 photocatalyst application for degradation of 4-chlorophenol. J Hazard Mater 252:233–242

[40] Liu N, Wang XZ, Xu WY, Hu H, Liang JJ, Qiu JS (2014) Microwave-assisted synthesis of MoS_2/grapheme nanocomposites for efficient hydrodesulfurization. Fuel 119:163–169

[41] Guo JH, Watanabe SG, Janik MJ, Ma XL, Song CS (2010) Density functional theory study on adsorption of thiophene on TiO_2 anatase (001) surfaces. Catal Today 149:218–223

[42] Qiu JH, Wang GH, Zeng DL, Tang Y, Wang M, Li YJ (2009) Oxidative desulfurization of diesel fuel using amphiphilic quaternary ammonium phosphomolybdate catalysts. Fuel Process Technol 90:1538–1542

[43] Li C, Jiang ZX, Gao JB, Yang YX, Wang SJ, Tian FP, Sun FX, Sun XP, Ying PL, Han CG (2004) Ultra-deep desulfurization of diesel: oxidation with a recoverable catalyst assembled in emulsion. Chem Eur J 10:2277–2280

[44] Lv HY, Li PC, Liu YM, Hao LW, Ren WZ, Zhu WJ, Deng CL, Yang F (2017) Synthesis of a hybrid Anderson-type polyoxometalate in deep eutectic solvents (DESs) for deep desulphurization of model diesel in ionic liquids (ILs). Chem Eng J 313:1004–1009

[45] Nisar A, Zhuang J, Wang X (2011) Construction of amphiphilic polyoxometalate mesostructers as a highly efficient desulfurization catalyst. Adv Mater 23:1130–1135

[46] Komintarachat C, Trakarnpruk W (2006) Oxidative desulfurization using polyoxometalates. Ind Eng Chem Res 45:1853–1856

[47] Duncan DC, Chmbers RC, Hecht E, Hill CL (1995) Mechanism and dynamics in the $H_3[PW_{12}O_{40}]^-$ catalyzed selective epoxidation of terminal olefins by H_2O_2. Formation, reactivity and stability of $\{PO_4[WO(O_2)_2]_4\}^{3-}$. J Am Chem Soc 117:681–691

[48] Ding YX, Zhu WS, Li HM, Jiang W, Zhang M, Duan YQ, Chang YH (2011) Catalytic oxidative desulfurization with a hexatungstate/aqueous H_2O_2/ionic liquid emulsion system. Green Chem 13:1210–1216

[49] Fatima M, Luis D, Mariana S, Ribeiro SO, Corvo MC, Castro B, Granadeiro CM, Balula SS (2018) Efficient heterogeneous polyoxometalate-hybrid catalysts for the oxidative desulfurization of fuels. Catal Commun 104:1–8

[50] Lv HY, Deng CL, Ren WZ, Yang X (2014) Oxidative desulfurization of model diesel using $[(C_4H_9)_4N]_6Mo_7O_{24}$ as a catalyst in ionic liquids. Fuel Process Technol 119:87–91

[51] Lv HY, Wang SN, Deng CL, Ren WZ, Guo BC (2014) Oxidative desulfurization of model diesel via dual activation by a protic ionic liquid. J Hazard Mater 279:220–225

[52] Noyori R, Aoki M, Sato K (2003) Green oxidation with aqueous hydrogen peroxide. Chem Commun. https://doi.org/10.1039/B303160H

[53] Zhu WS, Dai BL, Wu PW, Chao YH, Xiong J, Xun SH, Li HP, Li HM (2015) One-pot extraction combined with metal-free photochemical aerobic oxidative desulfurization in deep eutectic solvent. ACS Chem Eng 3:186–194